EPJ Web of Conferences **140**, 03065 (2017) DOI: 10.1051/epjconf/201714003065
Powders & Grains 2017

Effect of cohesion on local compaction and granulation of sheared soft granular materials

Sudeshna Roy[1,⋆], *Stefan* Luding[1,⋆⋆], and *Thomas* Weinhart[1,⋆⋆⋆]

[1]*Multi Scale Mechanics (MSM), MESA+, CTW, University of Twente, PO Box 217, 7500 AE Enschede, The Netherlands*

Abstract. This paper results from an ongoing investigation of the effect of cohesion on the compaction of sheared soft wet granular materials. We compare dry non-cohesive and wet moderately-to-strongly cohesive soft almost frictionless granular materials and report the effect of cohesion between the grains on the local volume fraction. We study this in a three dimensional, unconfined, slowly sheared split-bottom ring shear cell, where materials while sheared are subject to compression under the confining weight of the material above. Our results show that inter-particle cohesion has a considerable impact on the compaction of soft materials. Cohesion causes additional stresses, due to capillary forces between particles, leading to an increase in volume fraction due to higher compaction. This effect is not visible in a system of infinitely stiff particles. In addition, acting oppositely, we observe a general decrease in volume fraction due to increased cohesion for frictional particle, which we attribute to the role of contact friction that enhances dilation.

1 Introduction

Unsaturated granular media of particles with interstitial liquid in the form of bridges between particle pair, display bulk cohesion, which can be tuned using different liquids with varying surface tension. Earlier studies have been on density correlation in terms of fractal structure of aggregates for dry cohesive powders [1]. Cohesive grains being sensitive to stress intensity as well as direction exhibit much larger variations in their equilibrium densities. Moreover, adhesion would enhance the role of sliding and rolling friction, because the limiting values for tangential contact forces and rolling moments are both proportional to the elastic repulsive part of the normal force. Fournier et al. [2] observed that wet granulates are significantly less densely packed than dry granular materials, but the packing densities in only weakly dependent on the amount of wetting liquid, an obvious reason being that the forces exerted by the liquid bridges are very weakly dependent on bridge volume [3]. At small liquid content and after sufficient equilibration, the interior of the wet granulate is expected to be characterized by a network of liquid bridges connecting adjacent grains. It is clear that the connectivity of this network of liquid bridges is of importance for the mechanics of the wet granular materials, be it directly due to the capillary forces itself or due to the enhancement of the mutual friction between the grains by the increased internal pressure. For the wet granular materials, this pressure increase is of the order $\Delta p \approx \sigma/r$ given by the Laplace-Young equation, where r is a typical radius of the grains and σ is the surface tension of liquid. The local volume fraction of the bulk on macro-scale is connected to the pressure gradient and is thus proportional to σ.

We study here the packing fraction in the critical state for non-cohesive to strongly cohesive systems by varying the surface tension of the liquid. Details of the simulation set-up is given in Sec. 2.1. Wet granular materials are cohesive and particles can stick together and form local agglomerates or granules, due to formation of clusters of particles for very cohesive systems, as shown in figure 1 and 4(c). Figure 1 shows the top view of the split bottom shear cell geometry with colors blue to red indicating z coordinate values of the particles. It is observed from the figure that some particles form clumps near the surface while the particles near the base are seen through the hollow region. Hence, the system is highly inhomogeneous in its spatial distribution.

2 Model System

2.1 Geometry

Split-Bottom Ring Shear Cell: We use MercuryDPM [4, 5], an open-source implementation of the Discrete Particle Method, to simulate a shear cell with annular geometry and a split bottom plate, as explained in [6]. Earlier studies used similar rotating set-ups, including [7, 8]. The geometry of the system consists of an outer cylinder (radius R_o = 110 mm) rotating around a fixed inner cylinder (radius R_i = 14.7 mm) with a rotation frequency of $\Omega = 2\pi f$ and $f = 0.01$ revolutions per second. The granular material is confined by gravity between the two concentric cylinders and the bottom plate, with a free top surface.

⋆e-mail: s.roy@utwente.nl
⋆⋆e-mail: s.luding@utwente.nl
⋆⋆⋆e-mail: t.weinhart@utwente.nl

© The Authors, published by EDP Sciences. This is an open access article distributed under the terms of the Creative Commons Attribution License 4.0 (http://creativecommons.org/licenses/by/4.0/).

The bottom plate is split at radius R_s = 85 mm. Due to the split at the bottom, a narrow shear band is formed. It moves inwards and widens towards the flow surface. This set-up thus features a wide shear band away from the bottom and the wall which is free from boundary effects. The shear cell is filled up to a height of $H \approx 40$ mm under dry conditions, with particles of mean diameter $d_p = \langle d \rangle \approx 2.2$ mm, polydispersity $d_{\max}/d_{\min} = 2.0$ and gaussian distribution with width of $1 - \langle d \rangle / \langle d^2 \rangle = 0.0357$, where a is the particle radius. Thus, the shear band remains far away from the inner wall. The inter-particle friction coefficient is $\mu_p = 0.01$ and other parameters are detailed in [6].

In earlier studies [9], a quarter of this system ($0° \leq \phi \leq 90°$) was simulated using periodic boundary conditions. In order to save computation time, here we simulate only a smaller section of the system ($0° \leq \phi \leq 30°$) with appropriate periodic boundary conditions in the angular coordinate, unless specified otherwise. We have observed no noticeable effect on the macroscopic behavior in comparisons between simulations done with a smaller (30°) or larger (90°) opening angle. Note that for very strong attractive forces, the system becomes inhomogeneous and looses its radial symmetry: i.e. agglomeration of particles occurs. Then, particles interact on a larger length scale and thus the above statement is not true anymore.

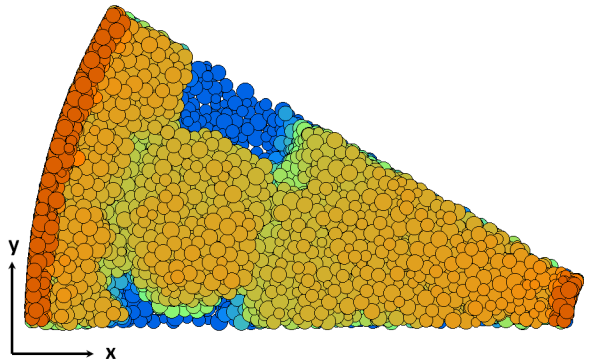

Figure 1: Top view of highly cohesive wet granular materials ($Bo_g = 34.6$). Different colors are the measure of low (blue), medium (green), high (yellow) and walls (red) z-coordinate of the particles.

2.2 Contact model and parameters

We use a linear visco-elastic frictional contact model in combination with Willet's capillary bridge model [3, 6, 10]. In order to see the effect of varying cohesive strength on the macroscopic rheology of wet materials, we vary the intensity of the maximum capillary force $f_{\text{cap}}^{\max} = \pi d \sigma \cos\theta$, by varying the surface tension of the liquid σ, while keeping the volume of liquid bridges constant, (V_b = 75 nl), corresponding to a liquid saturation of 8% of the voidage. We compare here the volume fractions of non-cohesive to moderate to strongly cohesive granular materials, with surface tension of liquid ranging from $\sigma = 0$ Nm^{-1}, up to $\sigma = 5$ Nm^{-1} for strongly cohesive systems. The contact angle is fixed at $\theta = 20°$.

3 Dimensionless numbers

The effects of varying shear rate, pressure, stiffness and cohesion can be modelled using three dimensionless numbers, expressed as a ratio of time-scales as given in Tab. 1, where the subscripts $\dot{\gamma}, p, k$ and c denote strain-rate, pressure, stiffness and cohesion respectively [10]. In addition, we define the *global* Bond number as $Bo_g = f_{\text{cap}}^{\max}/(p_{\text{mean}} {d_p}^2)$, where p_{mean} is the mean pressure in the system (at about half filling height $H/2$).

Table 1: Dimensionless numbers for the model

Dimensionless number	Definition	Time scale ratios
Inertial number I	$\frac{\dot{\gamma} d_p}{\sqrt{p/\rho}}$	$t_p/t_{\dot{\gamma}}$
Softness p^*	$\frac{p d_p}{k}$	$(t_k/t_p)^2$
Local Bond number Bo	$\frac{f_{\text{cap}}^{\max}}{p {d_p}^2}$	$(t_p/t_c)^2$

4 Rheological model

The macroscopic quantities are obtained by spatial coarse graining with temporal averaging of the system in steady state as detailed in [6, 10]. We study the effect of the above mentioned dimensionless numbers on the local volume fraction ϕ in the critical state [10]. The local volume fraction is expected to be dependent on various factors like the dilation, compression and the inter-particle friction. In the following sections, we discuss more of the effect of each dimensionless number on the local volume fraction.

4.1 Non-cohesive granular materials

For dry granular materials, $Bo = 0$, the rheology only depends on p^* and I. The dependence of the macroscopic friction coefficient $\mu = \tau/p$ on p^* and I has been studied in [9, 10]. In order to complete the rheology for soft, compressible particles, a relation for the solid volume fraction (packing fraction) as function of pressure and shear rate is missing for dry non-cohesive materials. In [11], the following dependency was observed:

$$\phi(I, p^*) = \phi_o f_I(I) f_p(p^*) \tag{1}$$

with the critical or steady state density under shear, first order i.e., in the limit of vanishing pressure and inertial number, $\phi_o = 0.64$, $f_p(p^*) = (1 + p^*/{p_o}^*)$, $f_I(I) = (1 - I/I_o)$. The typical strain rate for which dilation would turn to fluidization is $I_o = 0.85$, and the typical pressure level for which softness leads to huge densities is ${p_o}^* = 0.33$ [11]. Note that both correction functions are first order, i.e. they are valid only for sufficiently small arguments. Because of slow quasistatic flows in our simulations, no strong dilation is observed, i.e., no strong dependence of ϕ on the local shear rate. On the other hand, too large inertial numbers would fully fluidize the system so that the rheology should be that of a granular fluid, for which kinetic theory applies, while too large pressure would lead to enormous overlaps, for which the contact model and the particle simulation with pair forces become questionable.

4.2 Cohesive granular materials

In cohesive flows, attractive forces enhance the local stresses acting on the particles and adds an attractive force which acts as an effective confinement and increased compression, i.e. increased volume fraction (at least for our nearly-frictionless spheres). Rough and frictional particles should display stronger dilatancy, a reduced volume fraction under shear. Having low inter-particle friction, we observe an overall increase in local volume fraction with Bo (plot not shown here). This overall effect is distinguished as contribution from compression of soft particles and due to structural changes in presence of friction as discussed in the following subsections.

4.2.1 Effect of cohesion on soft particles

In cohesive flows, cohesion enhances the compressive pressure acting on the particles. This can be quantified as follows: we split the net pressure into two components, $p = p_{\text{rep}} - p_{\text{cap}}$, denoting the respective contributions of repulsive and cohesive contact forces. The ratio between the total cohesive contribution and the total pressure is given by the local bond number, $Bo = p_{\text{cap}}/p$, and thus $p_{\text{rep}} = (1 + Bo)p$. As the geometrical compression (deformation at each contact) is related to the *repulsive* stress, it is the compressive pressure p_{rep} that has to be considered in the softness factor f_p. Thus, the modified local softness correction for cohesive systems is given as:

$$f_p(p^*_{\text{rep}}) = f_p((1 + Bo)p^*) \tag{2}$$

For dry non-cohesive system when $Bo = 0$, one has $f_p((1 + Bo)p^*) = f_p(p^*)$. This is similar in spirit with the modified inertial number as presented in [12], which takes into account the cohesive contribution in effective stress. A similar modification in the inertial number is also required in the inertial regime weakly effective in the quasistatic regime.

4.2.2 Generalized effect of cohesion

In addition to the effect of cohesion on the softness of particles, cohesion also changes the microstructure [1, 2] in presence of rolling and sliding friction. To study this additional effect, we analyse the local packing fraction ϕ scaled by f_I and f_p as a function of the local Bond number Bo as shown in figure 2. All the data shown in figure 2 correspond to the critical state, though a shear band is not clearly defined in strongly cohesive systems ($Bo_g > 3.46$). It is observed from figure 2 that all data for different Bo_g collapse, following a trend and the dependence is given by the solid line in figure 2 as:

$$f_c(Bo) = \left[1 - \left(\frac{Bo}{Bo_c}\right)^{\alpha}\right] \tag{3}$$

where, $\phi_o = 0.65, \alpha = 0.57$ and $Bo_c = 729$ denotes the limiting Bond number above which the correction is not applicable anymore. The dash-dotted line represents a linear fit $f_c^{\text{lin}}(Bo)$ that ignores the larger Bo data, with $\alpha = 1$. Note that due to different friction $\mu_p = 0.5$, $\phi_o = 0.60, \alpha = 0.71$ and $Bo_c = 42.63$ for the dashed fit in figure 2 corresponding to the data from [13] for frictional monodisperse particles.

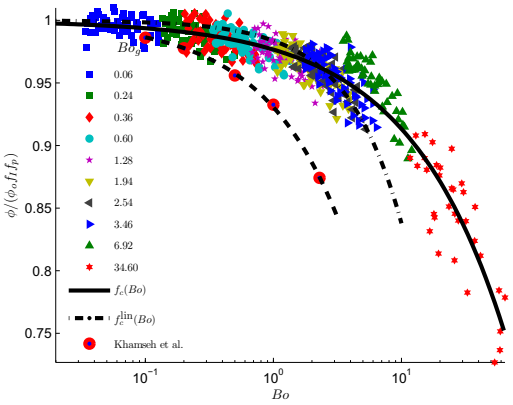

Figure 2: Scaled local packing fraction $\phi/(\phi_o f_I f_p)$ as a function of the local Bond number Bo showing the general decrease in scaled local volume fraction with cohesion. The solid line is given by Eq. (3) with parameters given in Tab. 2. The dash-dotted line corresponds to a simple linear fit $f_c^{\text{lin}}(Bo) = 1 - Bo/62$ corresponding to the data with $Bo < 3$. The dashed line corresponds to the fit for the data from [13].

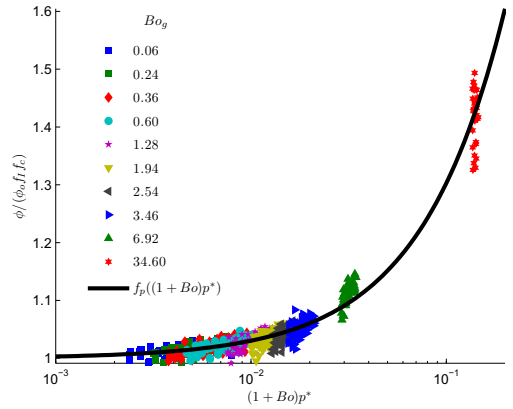

Figure 3: Scaled local packing fraction $\phi/(\phi_o f_I f_c)$ as a function of $(1 + Bo)p^*$ showing the effect of compaction of soft particles with increasing cohesion.

To confirm the effect of cohesion on the compressibility of soft particles, we re-plot figure 2 in another possible way, i.e., $\phi/(\phi_o f_I f_c)$ as a function of $(1 + Bo)p^*$ as shown in figure 3. In a way, this is the effect of compression of soft particles with increasing cohesion which is given by the function $f_p((1 + Bo)p^*)$ as shown by the solid line in the figure.

Thus the complete rheology for the local volume fraction is given as:

$$\phi(I, p^*, Bo) = \phi_o f_I(I) f_p((1 + Bo)p^*) f_c(Bo) \tag{4}$$

In the case of rigid particles, $p^* \to 0$ so that Eq. 4 reduces to $\phi_{\text{stiff}} = \phi(I, 0, Bo) = \phi_o f_I f_c$.

Table 2: Coefficients for the model

Dimensionless number	Corrections	Coefficients
Critical volume fraction (ϕ_o)		$\phi_o = 0.65$
Inertial number (I)	$f_I = \left(1 - \frac{I}{I_o}\right)$	$I_o = 0.85$
Softness (p^*_{rep})	$f_p = \left[1 + \frac{p^*_{\text{rep}}}{p_o{}^*}\right]$	$p_o{}^* = 0.33$
Cohesion (Bo)	$f_c = \left[1 - \left(\frac{Bo}{Bo_c}\right)^{\alpha}\right]$	See Sec. 4.2.2.

4.2.3 Discussion

Cohesion can either contribute to a decrease or an increase in the local volume fraction of sheared materials, depending on the inter-particle friction and the softness of materials. Note that compression is prevailing for soft particles but is negligible when $p^* > 0$ in the limit of infinite stiffness, when the local volume fraction is expected to increase with Bo. Berger et al. [12] uses contact dynamics for simulation which assumes that particles are infinitely stiff. Khamseh et al. [13] also shows that the volume fraction decreases for higher cohesion where the simulations are done using DEM with very stiff glass beads of Young modulus $E = 70$ GPa, so that for both, the softness effect is negligible.

Figure 4 (a), (b) and (c) show the contour plot of the spatial distribution of local packing fraction with the magnitude given by the color map for different $Bo_g = 0, 1.94$ and 34.6, respectively. Focusing on the shear band center, the mean volume fraction is close to 0.65 for non-cohesive materials as shown in figure 4(a). In comparison, the mean volume fraction of the strongly cohesive materials is 0.75 in figure 4(c). The vertical center of mass of the materials decreases by 25% from non-cohesive (a) to strongly cohesive (c) materials.

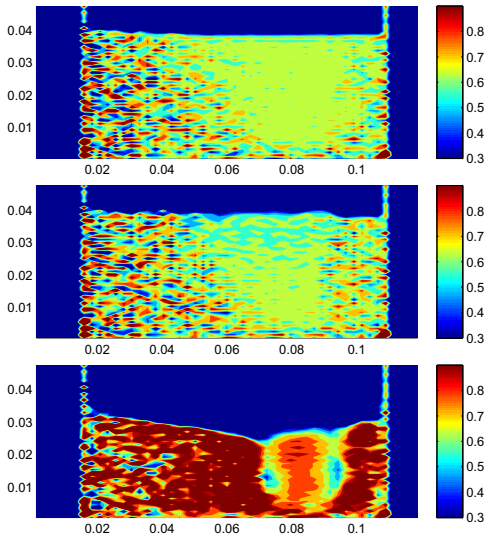

Figure 4: Contour plot of volume fraction for (a) $Bo_g = 0.0$, (b) $Bo_g = 1.94$ and (c) $Bo_g = 34.6$ in the $r - z$ plane. Both (a) and (b) are homogeneous in cylindrical direction, while (c) displays granule formation as shown in figure 1.

5 Conclusion

We studied the local packing fraction of dry and wet granular materials as a function of dimensionless numbers, namely, the inertial number I, the softness p^* and the Bond number Bo. Focus is on the effect of cohesion (quantified by the Bond number). Earlier studies have shown that the packing fraction of dry granular materials is to the first order linearly dependent on I and p^*.

We observe that the cohesive stress contributes to the softness for wet granular materials. This leads to an additional linear increment of local volume fraction with Bo. This effect is prevailing for soft particles and becomes negligible in the limits of stiff particles. Additionally, the local volume fraction decreases as a power law dependence on the local Bond number Bo. This is a more general effect of Bo on the local volume fraction related to the structural changes and increasing friction force of the materials.

Our results show that for strongly cohesive systems, our almost frictionless materials are overall densely compacted and center of mass of the bed drops by approximately 25%. The coordination number increases with local volume fraction. However, the trends are not clear enough and to have a complete understanding of the rheology, the dependence of the coordination number and the granular temperature on p^*, I and Bo should be studied.

Acknowledgements

We acknowledge our financial support through Technologiestichting STW Project 12272.

References

[1] F.A. Gilabert, J.N. Roux, A. Castellanos, Phys. Rev. E **75**, 11303 (2007)
[2] Z. Fournier, D. Geromichalos, S. Herminghaus, M.M. Kohonen, F. Mugele, M. Scheel, M. Schulz, B. Schulz, C. Schier, R. Seemann et al., J. Phys.: Condens. Matter **17**, S477 (2005)
[3] C.D. Willett, M.J. Adams, S.A. Johnson, J. Seville, Langmuir **16**, 9396 (2000)
[4] A. Thornton, T. Weinhart, S. Luding, O. Bokhove, Int. J. Mod. Phys. C **23, 124001** (2012)
[5] T. Weinhart, A. Thornton, S. Luding, O. Bokhove, Granul. Matter. **14**, 289 (2012)
[6] S. Roy, A. Singh, S. Luding, T. Weinhart, Computational Particle Mechanics **3**, 449–462 (2016)
[7] X. Wang, H.P. Zhu, A.B. Yu, Granular Matter **14**, 411 (2012)
[8] E. Woldhuis, B.P. Tighe, W. Saarloos, The European Physical Journal E: Soft Matter and Biological Physics **28**, 73 (2009)
[9] A. Singh, V. Magnanimo, K. Saitoh, S. Luding, New J. Phys. **17**, 043028 (2015)
[10] S. Roy, S. Luding, T. Weinhart, New Journal of Physics (accepted) (2017)
[11] S. Luding, A. Singh, S. Roy, D. Vescovi, T. Weinhart, V. Magnanimo, The 7th International Conference on Discrete Element Methods. (2016)
[12] N. Berger, E. Azéma, J.F. Douce, F. Radjai, EPL (Europhysics Letters) **112**, 64004 (2016)
[13] S. Khamseh, J.N. Roux, F. Chevoir, Physical Review E **92**, 022201 (2015)